Texture Analysis for Mars Rover Images

Rebecca Castaño, Tobias Mann and Eric Mjolsness

Jet Propulsion Laboratory, California Institute of Technology
4800 Oak Grove Drive, Pasadena, CA

ABSTRACT

The problem addressed in this paper is that of clustering image pixels into regions of homogenous geological texture. Future rovers on Mars will need to be able to intelligently select data collection targets. One goal of intelligent data selection for maximizing scientific return is to sample all distinct types of rocks that may be encountered. Different rock types often have a characteristic visual texture, thus visual texture is a rich source of information for separating rocks into different types.

Recent work on using texture to segment images has been very successful on images with homogenous textures such as mosaics of Brodatz textures and some natural scenes. The geologic history of a rock leads to irregular shapes and surface textures. As a result, the textures in our images are not as homogeneous as those in Brodatz mosaics.

Our approach is to extract textural information by applying a bank of Gabor filters to the image. The resulting texture vectors are then clustered. Banks of filters constrain the relationships of the filter parameters both within a single filter and between filters. Often researchers have used parameter values that are thought to correspond to the human visual system, however the effects of adjusting these parameters have not been thoroughly studied. We systematically explore tradeoffs in the parameter space of the filter bank and quantify the effects of the tradoffs on the quality of the resulting clusters.

Keywords: texture analysis, Gabor filters

1. INTRODUCTION

The amount of data that can be returned from interplanetary missions is much smaller than the amount of data that can be gathered by the instruments on those missions. One strategy for dealing with this bottleneck is to design systems that can intelligently select the data to be transmitted. To this end, at JPL we are working on a texture segmentation system that will allow rovers on Mars to choose rocks to examine based on visual texture. Visual texture can provide valuable clues to both the mineral composition and geological history of a rock, each of which is important to geologists. We use a set of Gabor filters to determine the features associated with each image pixel. Gabor filters are both scale and orientation specific, properties that make them suitable for use in discriminating between different textures.

Gabor filters have been popular for texture segmentation for many years in part due to the theory proposed by Daugman[1] that some simple cells in the visual cortex can be modelled by 2D Gabor functions. The use of Gabor functions for texture segmentation can be divided into two categories of application. In the first approach a bank of filters with fixed parameters is used to segment an image of unknown textures. In the second approach, one or a small set of filters are carefully designed to solve a specific problem, usually with a set of textures known a priori. Examples of the latter approach include Bovik et. al.[3–5] who thoroughly analyzed the properties of selecting a small set Gabor filters for texture discrimination, Dunn et. al.[6] who examined the problem of selecting a single filter to discriminate between two textures and Weldon et. al.[7,8] who looked at the problem of selecting one or a small set of Gabor filters to maximize discrimination between multiple known textures.

As we cannot anticipate all of the textures that may be encountered by a rover on Mars, we adopt the former approach. Parameter selection is an important issue with a bank of filters as well as with a smaller filter set. Jain and Farrokhnia[2] used a bank of filters with parameters selected based on computational considerations along with experimental evidence of the visual cortex. In another study of filter parameters, Lee[9] derived the conditions under which a set of Gabor wavelet filters provide a complete representation of an image. In this paper we emprically

Further author information: Rebecca.Castano@jpl.nasa.gov

explore the effects of varying several of the Gabor filter parameters on the quality of resulting classifications. We do not restrict filters to model the behavior of the visual cortex, to be independent, or to form a complete set.

We begin in Section 2 by presenting the mathematical formulation of a Gabor filter and discussing the relationship of filters within a bank. We then describe the parameters that we vary and how the rest of the parameters for a filter are derived. In our experiments we have compared the results of clustering the filter outputs to a ground truth. We explain the method we use for quantitatively assessing the agreement between two classifications in Section 4, and present experimental results in Section 5. Finally, in Section 6 we summarize our findings and discuss future directions for this research.

2. CHARACTERIZATION OF GABOR FILTERS

A Gabor function is a complex exponential modulated by a Gaussian.

$$G(x,y,\xi_o,\nu_o,x_o,y_o,\rho,\theta,\sigma_x,\sigma_y) = \frac{1}{\sqrt{\pi\sigma\beta}} e^{-\left(\frac{(x-x_o)\cos\theta+(y-y_o)\sin\theta)^2}{2\sigma_x^2}+\frac{(x-x_o)\sin\theta+(y-y_o)\cos\theta)^2}{2\sigma_y^2}\right)} e^{j(\xi_o(x-x_o)+\nu_o(y-y_o)+\rho)} \tag{1}$$

The filter is centered at $(x = x_o, y = y_o)$ in the spatial domain and $(\xi = \xi_o, \nu = \nu_o)$ in the spatial frequency domain. The parameters σ_x and σ_y define the standard deviations along the axes of the Gaussian ellipse when oriented with the x-axis. The orientation of the modulating Gaussian is given by θ and the phase of a filter is given by ρ. Thus, there are eight degrees of freedom.

When a bank of filters is used, the parameters of an individual filter are related to those of other filters within the bank. Several assumptions are frequently made to constrain the relationships of the filter parameters.

- We plan to use only the magnitude of the filter output so we may center the filter at the spatial origin, $x_o = 0, y_o = 0$, and set the phase of the filter to zero, i.e. $\rho = 0$.
- We let the modulating Gaussian be oriented with the complex exponential plane wave. This leads to $\xi_o = \omega\cos\theta$ and $\nu_o = \omega\sin\theta$ or $\omega = \sqrt{\xi_o^2 + \nu_o^2}$ where ω is called the radial frequency.

The equation for a single Gabor filter then becomes

$$G(x,y,\theta,\omega,\sigma_x,\sigma_y) = \frac{1}{2\pi\sigma_x\sigma_y} e^{-\left(\frac{(x\cos\theta+y\sin\theta)^2}{2\sigma_x^2}+\frac{(x\sin\theta+y\cos\theta)^2}{2\sigma_y^2}\right)} e^{j\omega(x\cos\theta+y\sin\theta)}. \tag{2}$$

Taking the Fourier transform yields

$$\begin{aligned} \mathrm{G}(u,v,\theta,F,\sigma_x,\sigma_y) &= e^{-2\pi^2\left(\sigma_x^2(u\cos\theta+v\sin\theta-F)^2+\sigma_y^2(u\sin\theta+v\cos\theta)^2\right)} &(3)\\ &= e^{-2\pi^2\left(\sigma_x^2(u'-F)^2+\sigma_y^2(v')^2\right)} &(4)\end{aligned}$$

where $u' = u\cos\theta + v\sin\theta$, $v' = u\sin\theta + v\cos\theta$, and $F = \omega/2\pi$. We see that in the spatial frequency domain, the Gabor filter is simply a Gaussian with $\sigma_u = 1/(\sigma_x\pi)$ and $\sigma_u = 1/(\sigma_x\pi)$.

In addition to these relationships, many researchers add additional assumptions based on physiological findings.[9]

1. The aspect ratio $\frac{\sigma_y}{\sigma_x}$ of the modulating Gaussian is 2 : 1.
2. The half-amplitude radial bandwidth of the frequency response is about 1 to 1.5 octaves.

We address the relaxation of assumption (2), which has two components. The first component is the use of the half-amplitude as the point of reference for the radial bandwidth while the second component is the selection of a the range 1 to 1.5 octaves for the value of the bandwidth. By fixing the radial bandwidth, different sized images will require different numbers of distinct center frequencies or scales. As a result, the number of filters in a filter bank becomes a function of image size. In the next section, we show the derivation of a bank of filters such that the number of filters is fixed for arbitrary image sizes. This is achieved by fixing the number of scales as well as the lower and upper bounds for spatial frequency space filter coverage.

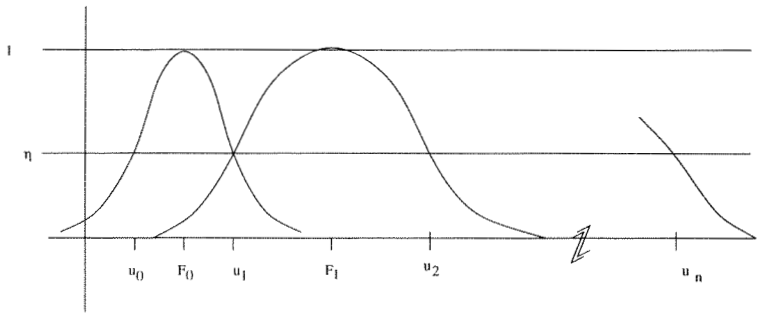

Figure 1. Cross section of Gabor filters centered on the u axis in the spatial frequency domain.

3. FILTER PARAMETER SELECTION

As was explained in the previous section, the filter bank will contain Gabor filters with four free parameters, θ, F, σ_x and σ_y. We now show how the individual filter parameters are determined by specifying five parameters for the entire bank of filtesr. These five parameters for the set of filters are the number of orientations, scales, minimum frequency, maximum frequency and overlap between filters of conscutive scales.

3.1. Orientation

Filter orientation, θ, can range from 0 to π. The orientation space is evenly sampled with each filter having angular bandwidth of π/N_θ where N_θ is the number of orientations sampled.

3.2. Center Frequency

The center frequencies, F, can be selected based on the number of radial scales along with the minimum and maximum frequency to be covered by the set of filters. Filter amplitudes along the $u = 0$ axis in the frequency domain for filters at different scales are shown in Figure 1. The filter radial center frequencies are spaced using a log scale. This means that the ratio of one filter center to the next is a constant, i.e.

$$\frac{F_i}{F_{i-1}} = 2^B \tag{5}$$

where B is the octave spacing of the center frequencies. Correspondingly, the radial filter widths are also related by

$$\frac{\sigma_{i_u}}{\sigma_{(i-1)_u}} = 2^B. \tag{6}$$

Given a minimum frequency, u_0, a maximum frequency, u_n, and the number of scales,n, we want to calculate the center frequencies for filters at each scale. The maximum value of each filter is one, so we do not normalize the area under the Gaussian. For a given filter along the u axis, we have

$$G(u) = e^{-\frac{1}{2}(u-F)^2/\sigma_u^2}. \tag{7}$$

We define the support, η, to be the height of the filter at the point where neighboring filters along the u axis intersect. In the past, most researchers have kept the support constant at 0.5. From Figure 1 we can see that

$$\eta = G_0(u_1) = e^{-\frac{1}{2}\frac{(u_1-F_0)^2}{\sigma_0^2}} = G_1(u_1) = e^{-\frac{1}{2}\frac{(u_1-F_1)^2}{\sigma_1^2}} \tag{8}$$

where we have dropped the subscript u from the parameter σ.

From Eq. (8) we have

$$\frac{(u_1 - F_o)^2}{\sigma_0^2} = \frac{(u_1 - F_1)^2}{\sigma_1^2} \tag{9}$$

and thus

$$u_1 = \frac{\sigma_0 F_1 + \sigma_1 F_0}{\sigma_0 + \sigma_1}. \tag{10}$$

Since $F_1 = 2^B F_0$ and $\sigma_1 = 2^B \sigma_0$ we have

$$u_1 = F_0 \left(\frac{2^{B+1}}{1 + 2^B} \right). \tag{11}$$

Using the same steps with F_1, F_2 and u_2 we arrive at

$$\begin{aligned} u_2 &= F_1 \left(\frac{2^{B+1}}{1 + 2^B} \right) \\ &= F_0 2^B \left(\frac{2^{B+1}}{1 + 2^B} \right). \end{aligned} \tag{12}$$

Similarly,

$$\begin{aligned} u_n &= F_n \left(\frac{2^{B+1}}{1 + 2^B} \right) \\ &= 2^{B(n-1)} F_0 \left(\frac{2^{B+1}}{1 + 2^B} \right). \end{aligned} \tag{13}$$

Solving Eq. (13) for F_0 gives

$$F_0 = u_n 2^{-B(n-1)} \left(\frac{1 + 2^B}{2^{B+1}} \right). \tag{14}$$

We have arrived at an expression for F_0 that involves u_n and B. At this point, however, the octave spacing between filter scales, B, is not known. We proceed to solve for B in terms of the known minimum and maximum frequencies, u_0 and u_n, by observing that $G_0(u_0) = G_{n-1}(u_n)$ which we can write as

$$e^{-\frac{1}{2}\frac{(u_0 - F_o)^2}{\sigma_0^2}} = e^{-\frac{1}{2}\frac{(u_n - F_{n-1})^2}{\sigma_{n-1}^2}}. \tag{15}$$

Substituting for F_{n-1} and σ_{n-1} we see that Eq. (15) yields

$$\frac{(F_0 - u_0)}{\sigma_0} = \frac{(u_n - 2^{B(n-1)} F_0)}{2^{B(n-1)} \sigma_0}. \tag{16}$$

After substituting Eq. (14) into Eq. (16) we can arrive to

$$\frac{u_n}{u_0} = 2^{Bn}. \tag{17}$$

Solving for B we get

$$B = \frac{\ln \frac{u_n}{u_0}}{n \ln 2} \tag{18}$$

which is our desired expression for B in terms of u_0 and u_n.

The center frequencies are thus calculated by first evaluating Eq. (18) followed by

$$F_0 = \frac{u_0}{2} \left(1 + 2^B \right) \tag{19}$$

in which Eq. (17) has been used to simplify Eq. (14). The rest of the frequencies follow using $F_i = 2^{B(i-1)} F_0$. We have thus shown how the radial center frequencies can be determined by specifying the number of scales, along with the minimum and maximum frequency coverage for the filter bank.

3.3. Filter Widths

The width of a filter in the radial direction is given by σ_u. Having determined the center frequencies as described in the previous section, we can solve Eq. (8) for $\sigma_0 = \sigma_{0_u}$. The resulting expression is

$$\sigma_{0_u} = -\frac{1}{2}\frac{(u_0 - F_0)^2}{\ln n}. \tag{20}$$

In general, the width of a filter at scale $i \in [2..n-1]$ is given by

$$\sigma_{i_u} = 2^{Bi}\sigma_{0_u}. \tag{21}$$

The width in the angular direction is obtained by solving

$$\tan\frac{\pi}{N_\theta} = \sqrt{\frac{-\ln\eta}{2}}\left(\frac{\sigma_{0_v}}{F_0}\right). \tag{22}$$

4. CLASSIFICATION

After the bank of Gabor filters is run over the image, we use k-means clustering to classify the pixels. We choose a number of clusters k appropriate for the image. There is no post-processing after the classification step.

Once the image features have been computed and clustered, the quality of the classification needs to be assessed in a quantitative way. For our geological images, we asked geologists to hand label a set of images so as to provide a reference classification. Several approaches have been used to compare two classifications. Perhaps the simplest is to compute the percentage of pixels which agree; however, a matching from one set of labels to the other must be computed and difficulties arise when the two labellings have a different number of classes. One case where percentage of agreement will fail to give a good measure of the quality of a clustering is where one of the reference classes is perfectly matched by the union of two of the classes found by the clustering algorithm; in this case the two classes could be merged, perhaps with some penalty, yielding a much better score. Another measure given by Congalton[11] is the KHAT statistic, which measures the agreement of the classification (again assuming the correspondence of the reference classes and the classes found by the clusterer is known or computed) and takes into consideration that the probability that the agreement occurred by chance.

The measure of quality we have chosen to use is the mutual information of the joint distributions given by the classifications. Given the joint distribution $p(x,y)$ and the marginal distributions $p(x)$ and $p(y)$ for all labels x in classification X and all labels y in classification Y, the mutual information[12] $I(X;Y)$ is

$$I(X;Y) = \sum_x \sum_y p(x,y) log \frac{p(x,y)}{p(x)p(y)} \tag{23}$$

The mutual information is a nonnegative quantity; we divide it by the mutual information given by the joint distribution of the reference classification with itself to get a score between 0 and 1.

5. EXPERIMENTAL RESULTS

The image analysis procedure is shown in Figure 2. Our set of test images includes two kind of images , images of geological interest and a mosaic of Brodatz textures of the kind often seen in texture classification research. The geological images consist of two kinds; in two images our task is to discriminate rock and sand, and in the other our task is to locate regions in the image with different pebble sizes. Segmenting the rocks by grayscale is possible in these images, but on mars there is a pervasive coating of red dust, reducing the contrast between the rocks and the soil; therefore, contrast is a less reliable feature than gross surface texture. Looking for grain size differences is relevant for understanding the sedimentary deposition; larger grains are associated with different deposition processes.

For our experiments, we chose a filterbank consisting of 20 filters consisting of 5 scales and 4 orientations. We report on a set of experiments where we vary the η parameter, since η affects the overlap of the filters in frequency space, and therefore the redundancy of the image features. Our results show that the value of η which gives the best classification varies widely among particular images. Figures 3-6 show our plots of mutual information as a function of η, and the classification that results from the optimal value of η for each image.

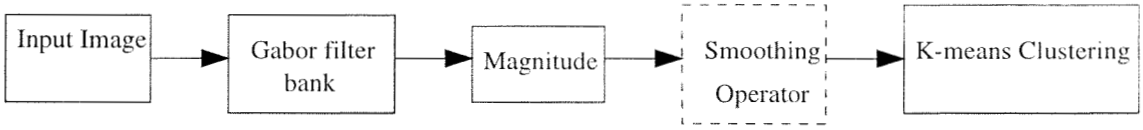

Figure 2. Texture analysis scheme. Optional processing steps are indicated with dashed lines.

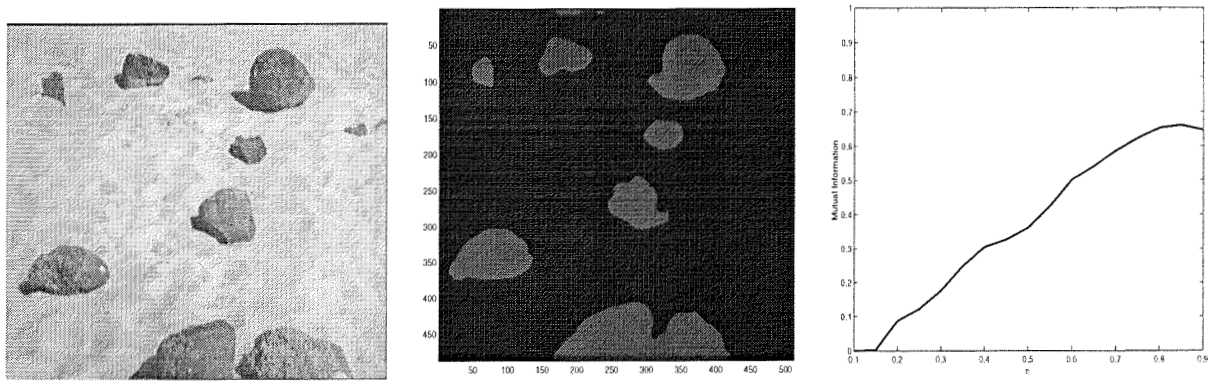

(a) (b) (c)

Figure 3. (a) original image (b) clustering result with $\eta = 0.85$ (c) mutual information scores for test images as overlap, η, is varied.

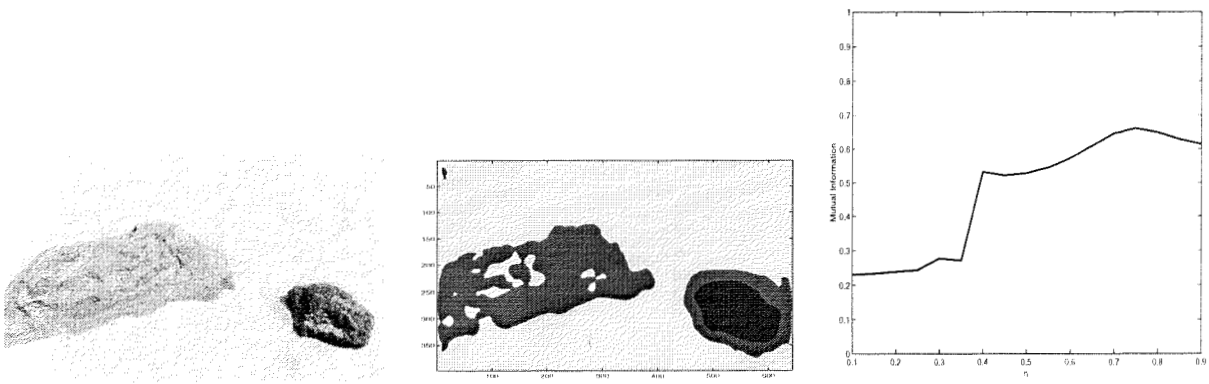

(a) (b) (c)

Figure 4. (a) original image (b) clustering result with $\eta = 0.75$ (c) mutual information scores for test images as overlap, η, is varied.

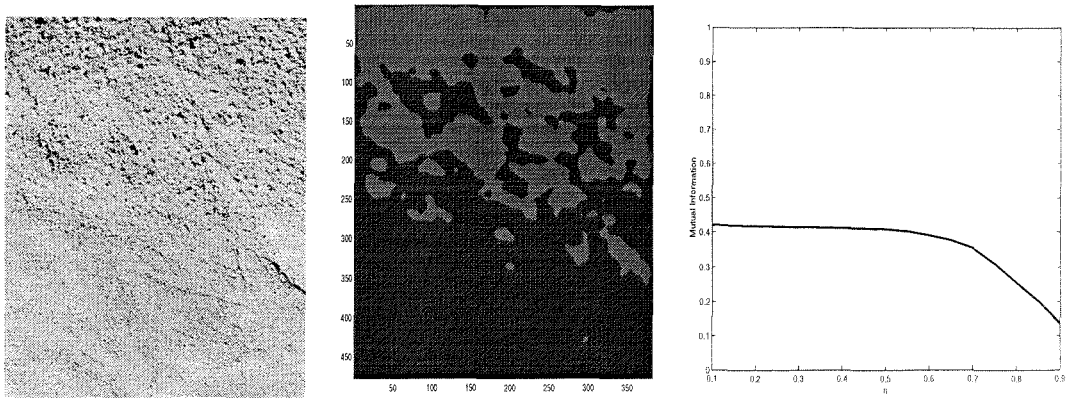

(a) (b) (c)

Figure 5. (a) original image (b) clustering result with $\eta = 0.1$ (c) Mutual information scores for test images as overlap, η, is varied.

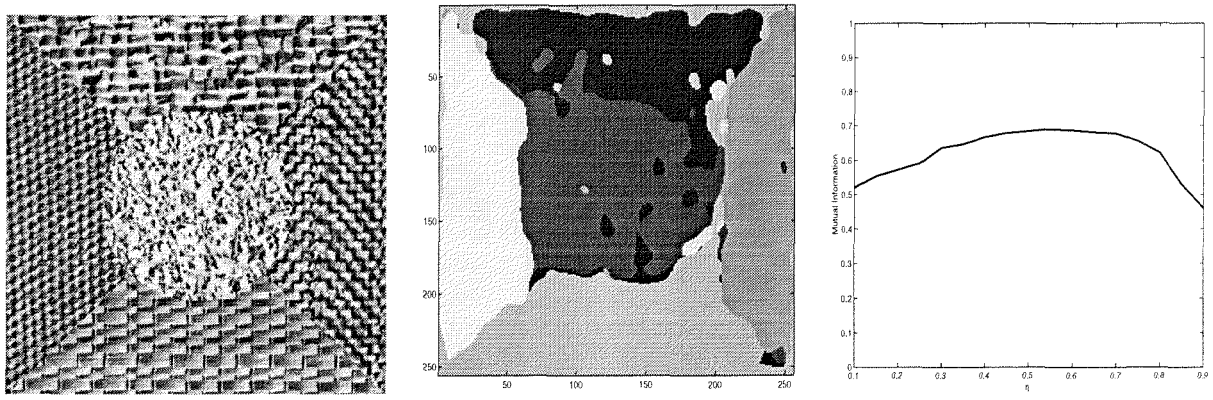

(a) (b) (c)

Figure 6. (a) original image [†] (b) clustering result with $\eta = 0.5$ (c) Mutual information scores for test images as overlap, η, is varied.

6. CONCLUSIONS

It is common in the texture literature to try to choose Gabor filter parameters which mimic the human perceptual system; however, our experiments show that parameters modeled on the human visual system are not optimal for all cases. The parameters that do well on a particular discrimination task depend on a range of factors, such as the imaging modality and the particular textures to be classified. Thus, with different parameters, Gabor filtering may yield better performance than was observed in the experiments performed by Randen et. al.[10] comparing a variety of texture segmentation methods. The parameters that work well for a particular imaging modality (such as the human perceptual system) are almost certainly not generally appropriate, and the parameters must be carefully chosen for the task at hand.

ACKNOWLEDGMENTS

This work was performed by the Jet Propulsion Laboratory, California Institute of Technology under contract with the National Aeronautics and Space Administration. This work was supported by the NASA Telerobotics Program

[†]Image provided by Trygve Randen, http://ux.his.no/~tranden

and the Remote Exploration and Experimentation Project. The texture mosaic image was provided by Trygve Randen from http://www.ux.his.no/~tranden.

REFERENCES

1. J. G. Daugman, "Uncertainty relation for resolution in space, spatial frequency, and orientation optimized by two-dimensional visual cortial filters," *J. Opt. Soc. Am. A* **2**(7), pp. 1160–1169, 1985.
2. A. K. Jain and F. Farrokhnia, "Unsupervised texture segmentation using Gabor filters," *Pattern Recognition* **23**(12), pp. 1167–1186, 1991.
3. A. C. Bovik, "Analysis of multichannel narrow-band filters for image texture segmentation," *IEEE Tran. Signal Processing* **39**(9), pp. 2025–2043, 1991.
4. A. C. Bovik, M. Clark, and W. S. Geisler, "Multichannel texture analysis using localized spatial filters," *IEEE Tran. Pattern Anal. Mach. Intel.* **12**(1), pp. 55–73, 1990.
5. M. Clark and A. C. Bovik, "Experiments in segmenting texton patterns using localized spatial filters," *Pattern Recognition* **22**(6), pp. 707–717, 1989.
6. D. Dunn, W. E. Higgins, and J. Wakely, "Texture segmentation using 2-D Gabor elementary functions," *IEEE Tran. Pattern Anal. Mach. Intel.* **16**(2), pp. 130–149, 1994.
7. T. P. Weldon and W. E. Higgins, "Multiscale Rician approach to Gabor filter design for texture segmentation," in *IEEE Int. Conf. Image Processing*, pp. 620–624, 1994.
8. T. P. Weldon and W. E. Higgins, "Design of multiple Gabor filters for texture segmentation," in *IEEE 1996 Int. Conf. Acoustics, Speech and Signal Processing*, pp. 7–10, 1996.
9. T. S. Lee, "Image representation using 2D Gabor wavelets," *IEEE Tran. Pattern Anal. Mach. Intel.* **18**(10), pp. 959–971, 1996.
10. T. Randen and J. H. Husoy, "Filtering for texture classification: A comparative study," *IEEE Tran. Pattern Anal. Mach. Intel.* **21**(4), pp. 291–310, 1999.
11. R. G. Congalton, "A review of assessing the accuracy of classifications of remotely senses data," *Remote Sensing of Environment* **37**(1), pp. 35–46, 1991.
12. J. Thomas and T. Cover, *Elements of Information Theory*, John Wiley & Sons, Inc., 1991.